https://doi.org/10.1016/j.jallcom.2022.166973

Efficient Electrocatalytic Nitrogen Reduction to Ammonia with FeNi-Co/Carbon Mat Electrodes

Yun Liu[a,1], Zhefei Pan[a,1], Oladapo Christopher Esan[a,], Xinhua Liu[b,*], Huizhi Wang[c,*], Liang An[a,d*]

[a] Department of Mechanical Engineering, The Hong Kong Polytechnic University, Hung Hom, Kowloon, Hong Kong SAR, China

[b] School of Transportation Science and Engineering, Beihang University, Kejiyuan Rd, Haidian, Beijing 100083, China

[c] Department of Mechanical Engineering, Imperial College London, Exhibition Road, London SW7 2AZ, United Kingdom

[d] The Hong Kong Polytechnic University Shenzhen Research Institute, Shenzhen 518057, China

[1] Equal contribution.

*Corresponding authors.

Email: liuxinhua19@buaa.edu.cn (Xinhua Liu)

Email: huizhi.wang@imperial.ac.uk (Huizhi Wang)

Email: liang.an@polyu.edu.hk (Liang An)

Abstract

Electrochemical nitrogen reduction reaction has recently received increasing attention due to its ability to synthesize ammonia under ambient conditions. However, the low ammonia yields and Faradaic efficiency hinder its further development, which necessitates the use of high-performance catalysts. Hence, in this study, a self-supporting carbon mat with FeNi-doped Co catalysts ($Co_{145}Fe_1Ni_{0.2}$) fabricated by electrospinning was used as an electrode (FeNi-Co@CM) for electrochemical ammonia synthesis. The electrochemical performance of the FeNi-Co@CM electrode is evaluated in a three-electrode setup with FeNi-Co@CM as working electrode, a platinum mesh as counter electrode, and a Ag/AgCl electrode as reference electrode. The experimental investigations produce an ammonia yield rate of 27.9 $\mu g\,h^{-1}\,mg^{-1}$ and a Faradaic efficiency of 1.52 % in 1.0 M KOH, which is higher than most of the reported data where iron-group-based electrocatalysts were employed. The verification results from multiple sets of control experiments indicated that the ammonia detected is generated by the nitrogen reduction reaction rather than the contaminants in the surrounding environment. In addition, the results of the stability test show that the FeNi-Co@CM electrode can maintain a high level of ammonia production for more than ten cycles. The working mechanism of nitrogen reduction reaction based on FeNi-Co@CM electrode is also discussed at various scales, including the electrode scale, the catalyst scale, and the atomic scale. This study therefore provides an in-depth understanding of the nitrogen reduction reaction from various perspectives, such as mass transport, reaction interfaces, and reaction intermediates.

Keywords: Ammonia synthesis; Nitrogen reduction reaction; Transition metals; Electrocatalyst; Faradaic efficiency; Ambient conditions

1. Introduction

Ammonia (NH_3), as one of the most important industrial chemicals in the world, can be used as fertilizer as well as fuel [1–3]. In recent years, ammonia has also been considered as a promising carrier of hydrogen (17.6 wt.%) with remarkable characteristics, such as high volumetric energy density (12.7 MJ/L), easy storage and transport (liquefaction temperature of -33 ºC at atmospheric pressure), and inherently carbon-free. Ammonia production currently relies on the Haber-Bosch method, which is an energy-intensive process involving high temperatures (300-500 ºC) and high pressures (150-300 atm), taking up 1-2% of the world's energy consumption and resulting in about 1% of the global CO_2 emissions [4]. These downsides of the conventional ammonia production technologies therefore necessitate the development of new ammonia production technologies. Recently, a promising strategy for the synthesis of ammonia via electrochemical nitrogen reduction reaction (NRR) has received much attention due to its capability to operate under ambient conditions [5]. However, electrochemical ammonia synthesis technology is currently limited by its inherently sluggish reaction kinetics and competing reactions (HER) [6]. As a result, the ammonia yield (~10^{-10} to 10^{-11} mol s^{-1} cm^{-2}) and Faraday efficiencies (~10%) currently achieved are well below the 10^{-6} mol s^{-1} cm^{-2} NH_3 yield and 90% FE targets set by the US Department of Energy (DOE) [7–9]. In order to achieve higher yield and Faradaic efficiency for electrochemical ammonia synthesis, researchers have been devoted to exploring and developing novel electrocatalytic materials with high selectivity and high activity for NRR in the past few decades [10–12]. Recently, noble metal materials and their related compounds have received continuous attention from materials scientists due to their excellent catalytic properties in various electrochemical reactions [13]. For example, Nazemi et al. [14] developed hollow gold nanocages as electrocatalysts and tested their NRR performance in H-cells with 0.5 M $LiClO_4$ aqueous solution as the electrolyte. The experimental results showed that high ammonia yield (3.9 mg h^{-1} cm^{-2}) and high Faraday efficiencies (30.2%) were obtained due to the increased surface area and the confinement of the reactants within their cavities (cage effect). In another study, Chung et al. [15] developed a Rh-based catalyst for the electrochemical synthesis of ammonia which exhibited an excellent NH_3 yield of 57.2 μg h^{-1} mg_{cat}^{-1} at -0.6 V vs. RHE and a high Faraday efficiency of 22% at -0.2 V vs. RHE in a 0.1 M Na_2SO_4 electrolyte. However, precious metals are expensive and limited reserves prevent them from being widely deployed and commercialized [16]. Therefore, it is imperative to develop catalyst materials with low costs and abundant reserves. Transition metal elements, such as iron, cobalt and nickel, which are characterized by their large reserves and low cost, have gained the attention of researchers and previous studies have shown that these transition metal materials are very promising electrocatalytic materials for NRR [17–19]. Among the different types of transition metal elements, cobalt is considered as a promising catalyst candidate for the electrochemical synthesis of ammonia because of its special electronic configuration ($3d^7 4s^2$) [20,21]. Chu et al. [22] developed a cobalt-based catalyst supported by reduced graphene oxide (RGO), demonstrating high ammonia yields of 21.5 μg h^{-1} mg^{-1} and a FE of 8.3%. Similarly, Wei et al. [23] designed CoS_2 nanoparticles as the NRR catalyst, exhibiting ammonia yields of 17.45 μg h^{-1} mg^{-1} and a FE of 4.6%. In recent years, scientists are increasingly interested in element-doped electrocatalysts for improving electrochemical performance by altering the morphology or conductivity of the catalyst through the inclusion of small amounts of additional elements [24,25]. It was demonstrated by Zhang et al. that FeNi bimetallic catalysts can greatly reduce the overpotential of electrochemical reactions, assisting in the improvement of electrochemical efficiency [26]. More importantly, previous studies have shown that the combination of different types of transition metals can synergistically enrich the local active catalytic site and change its electronic structure, thus contributing to the performance of electrochemical reactions [27].

Following these developments, a FeNi-Co@CM electrode fabricated by electrospinning is used for electrochemical ammonia synthesis under ambient conditions in this study. A detailed characterization of FeNi-Co@CM electrode material is first performed. Subsequently, electrochemical characterization is applied to test the ammonia production performance of the FeNi-Co@CM electrode. Following this, stability tests are conducted on the FeNi-Co@CM electrode to examine its durability. Various control experiments, including a potentiostatic test under argon bubbling, an open circuit voltage test etc., are also conducted to ensure that the ammonia detected in the experiment originated from the NRR . Finally, the mechanism of NRR is discussed at three different scales: the electrode scale, the catalyst scale, and the atomic scale, to provide a comprehensive understanding of the NRR from various perspectives, such as mass transport (transport of species, ions, and electrons), reaction interface, and reaction intermediates.

2. Experiment section

2.1 Material preparation and characterization

The synthesis process of the FeCo-Ni@CM electrode is briefly described as follows: three metal salts - $Fe(acac)_3$, $Ni(acac)_2$, and $Co(acac)_2$ powders are first mixed with polyacrylonitrile (PAN) such that the total mass in fraction of Fe and Ni metal salts is less than 1% to obtain the precursor solution. The precursor solution is then spun into a carbon fiber interwoven non-woven fabric, i.e., the electrode, by applying electrostatic spinning technology. To stabilize the structure, the electrode is first heated in air at 290 °C for two hours. The pre-treated electrode is then placed in a nitrogen atmosphere and heated at 850 °C for another two hours. In this way, the FeNi-Co@CM electrode can be synthesized. A detailed similar material preparation process has been demonstrated in our previous work [28].

The surface morphology of FeNi-Co@CM was observed using scanning electron microscopy (SEM) (Zeiss Sigma 300, Germany). The high-resolution transmission electron microscopy (HRTEM) images and high-angle annular dark-field-scanning transmission electron microscopic (HAADF-STEM) images were obtained using a JEM-2100F (JEOL, Ltd., Japan). The phase analysis of FeNi-Co@CM was conducted by X-ray diffraction (XRD) (D/max 2500PC) while the element analysis was conducted by energy-dispersive X-ray (EDX). The valence states of elements were analyzed by X-ray photoelectron spectroscopy (XPS), recorded by a spectrometer with Mg/Al Kα radiation (Thermo VG Scientific, USA). As for the detection of ammonia concentration in the test solution, the absorbance peak was measured using a UV-Vis double beam spectrophotometer (DB-20, Australia). The catalyst loading of the electrode was measured by inductively coupled plasma mass spectrometry (ICP-MS) (Agilent 7700x, USA).

2.2 Electrochemical measurements

A three-electrode electrochemical cell was used to evaluate the NRR performance of the FeNi-Co@CM electrode under ambient conditions, using FeNi-Co@CM (1.0 x 1.0 cm^2) as the working electrode with a catalyst loading of 0.146 mg cm^{-2}. A platinum mesh with a geometric surface area of 1.0 cm^2 was used as the counter electrode, and a Ag/AgCl electrode was used as the reference electrode. All the potentials were converted to a reversible hydrogen electrode (RHE) scale via calibration with the following equation [29]:

$$E_{(RHE)} = E_{Ag/AgCl} + 0.059\ pH + 0.1976 \tag{1}$$

0.059 was calculated from the Nernst equation while 0.1976 V was the value of $E^{o}_{Ag/AgCl}$ at 25 °C. 1.0 M KOH (115.0 mL) solution was used as the electrolyte as the K^+ has been proven to promote electrochemical NRR [30]. A Fumasep FAS-30 anion exchange membrane (Fuel Cell Store, USA) was employed to separate the anode and cathode compartments as well as to provide an anion transport path during the cell operation.

The experimental setup is shown in Fig. 1, including a nitrogen cylinder employed to provide the pure nitrogen (99.995%, 1.0 atm), an acid trap containing 0.05 M $H_2SO_{4(aq.)}$ and an alkaline trap containing 1.0 M $KOH_{(aq.)}$ to remove any possible ammonia and nitrogen oxides contaminants, a gas flowmeter to control the flow rate of nitrogen supply, a three-electrode electrochemical cell and an electrochemical workstation (M204, Switzerland) to conduct the electrochemical measurements, and another saturator filled with 0.05 M $H_2SO_{4(aq.)}$ to serve as an acid trap to capture any generated ammonia. A pictorial diagram of the electrochemical cell (H-cell) used for the experiments is presented in Fig. S1.

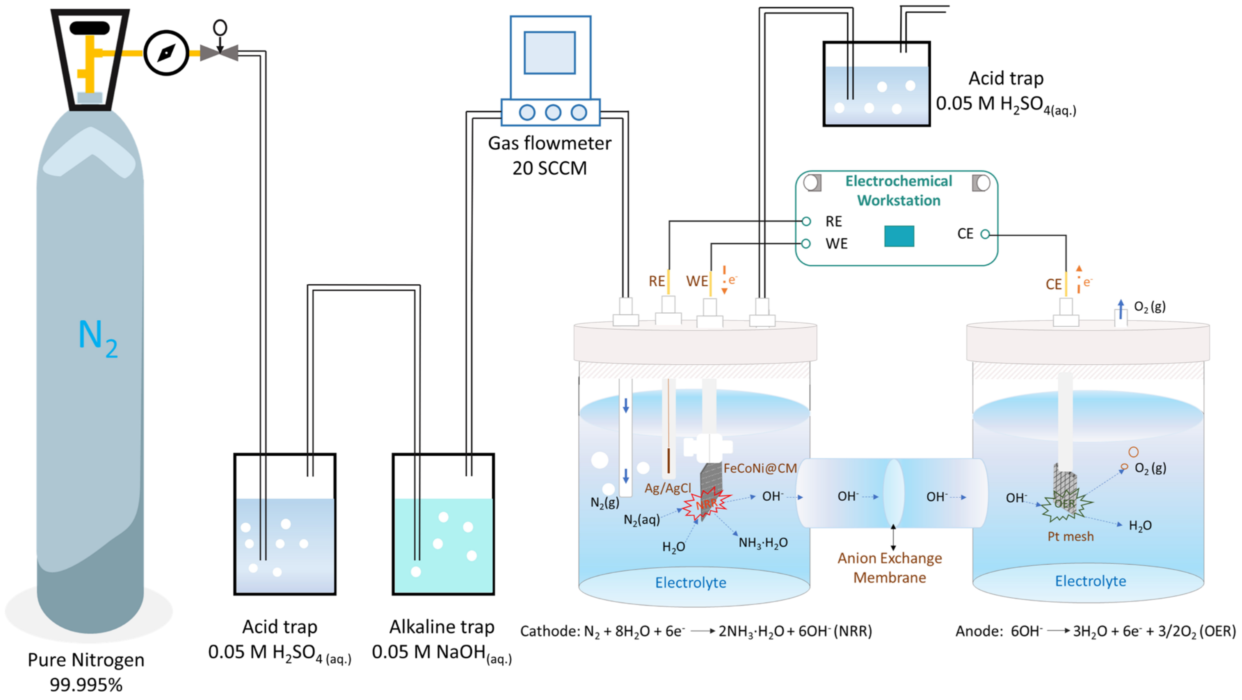

Fig. 1. Experimental setup for the electrochemical ammonia synthesis.

Before the electrochemical measurements, pretreatments were conducted on all the experimental setups and materials to avoid any contaminants that could affect the experimental results. The Fumasep FAS-30 anion exchange membrane was converted into OH^- form by soaking it in 1.0 M KOH solution for 24.0 h under ambient conditions, and then soaked in deionized water. All the components used in the experiment were thoroughly washed with deionized water to eliminate contaminants. Afterwards, 60 min of pure N_2 bubbling at a flow rate of 20 mL/min was first conducted to saturate the electrolyte and the cathode compartment. Furthermore, the electrolyte was constantly stirred at 200 rev/s during the cell operation to enable the dissolved nitrogen to be well dispersed in the electrolyte.

The linear sweep voltammetry (LSV) test was applied to determine whether the synthesized electrode has the function of synthesizing ammonia. The NRR and HER are the main electrochemical reactions that occur under N_2 bubbling conditions while HER is the main electrochemical reaction that occurs under Ar bubbling conditions. Following this consideration, a short-term chronoamperometry test was first applied in this work to measure the polarization curves under N_2 and Ar bubbling conditions [31]. After the potential window for effective electrochemical synthesis of ammonia was confirmed, the potentiostatic tests were conducted for 2.0 h in the N_2-saturated 1.0 M KOH solution with the continuous flowing of pure N_2 (99.99%). Besides, to verify the durability of the FeNi-Co@CM electrode, a stability test in terms of ammonia yield rates and FE was conducted. To further confirm that the detected ammonia originates from the electrochemical NRR on the FeNi-Co@CM electrode, two comparative experiments were conducted in which the electrochemical NRR was carried out in an Ar saturated solution and an N_2 saturated solution at an open-circuit potential.

2.3 Determination of ammonia and hydrazine

The ammonia concentration was measured by the indophenol blue method. For the preparation of the chromogenic solution, 1.0 mL electrolyte was taken from the cathodic chamber, and 1.0 mL of 1.0 M NaOH solution containing 5% salicylic acid and 5% sodium citrate was added to the solution. Subsequently, 0.5 mL of 0.05 M NaClO and 0.1 mL of 1% $C_5FeN_6Na_2O\cdot 2H_2O$ were added into the solution. After 2.0 h, the absorption spectrum of the mixed solution was measured by using a UV-visible spectrophotometer at a wavelength of 650 nm. The corresponding absolute calibration curve of standard NH_4Cl solution can be obtained by measuring the standard NH_4Cl solution with a series of known concentrations (0.25, 0.5, 1.0, 2.0, and 4.0 μg/mL). Therefore, a fitted curve ($y = 0.12837x + 0.00438$, $R^2 = 0.999$) between the absorbance and the ammonia concentration was developed (See Fig. S2).

The production of N_2H_4 in the electrolyte was evaluated by the Watt and Chrisp method. The color reagent for this method consists of 0.599 g of $C_9H_{11}NO$, 3.0 mL of calibration HCl (37 wt. %), and 30.0 mL of C_2H_5OH. During the process of detection, 1.0 mL electrolyte was taken from the cathodic chamber, adding 1.0 mL of the prepared color reagent and thereafter leave the solution for 20 min at room temperature. The absorbance at a wavelength of 457 nm was used to calculate the hydrazine concentration. The corresponding absolute calibration curve of standard $N_2H_4 \cdot H_2O$ solution was obtained using the standard $N_2H_4 \cdot H_2O$ solution with a series of known concentrations (0.125, 0.25, 0.5, 1.0, and 2.0 μg/mL). As a result, a fitted curve ($y = 0.94724x + 0.00467$) between the absorbance and the hydrazine concentration was established (see Fig. S2).

3. Results and discussion

3.1 Material characterization results

The surface morphologies of FeNi-Co@CM electrode are presented in Fig. 2, indicating that a unique electrode structure is obtained, in which the secondary carbon hairs are in situ grown on non-woven electrospun fibers. These fibers, with a diameter of about few hundred nanometers, are manufactured directly by electrospinning. In the case of secondary carbon hairs, the growth mechanism is demonstrated as follows: firstly, metal oxide nanoparticles are formed in the carbon fibers by metal salt additives during pre-carbonisation and then reduced to form metal domains after further heat treatment. Secondly, these metal nanoparticles diffuse onto the surface of the carbon fibers through an exsolution mechanism, resulting in nanoparticle-modified carbon fibers. Then, during the second carbonisation process, the PAN thermally decomposes to produce CH_4 and CO. These carbon-containing materials further decompose in situ to produce a new source of carbon [32], which is deposited on the surface of the nanoparticles and gradually forms the carbon hairs on the surface of the carbon fibers as shown in Fig. 2.

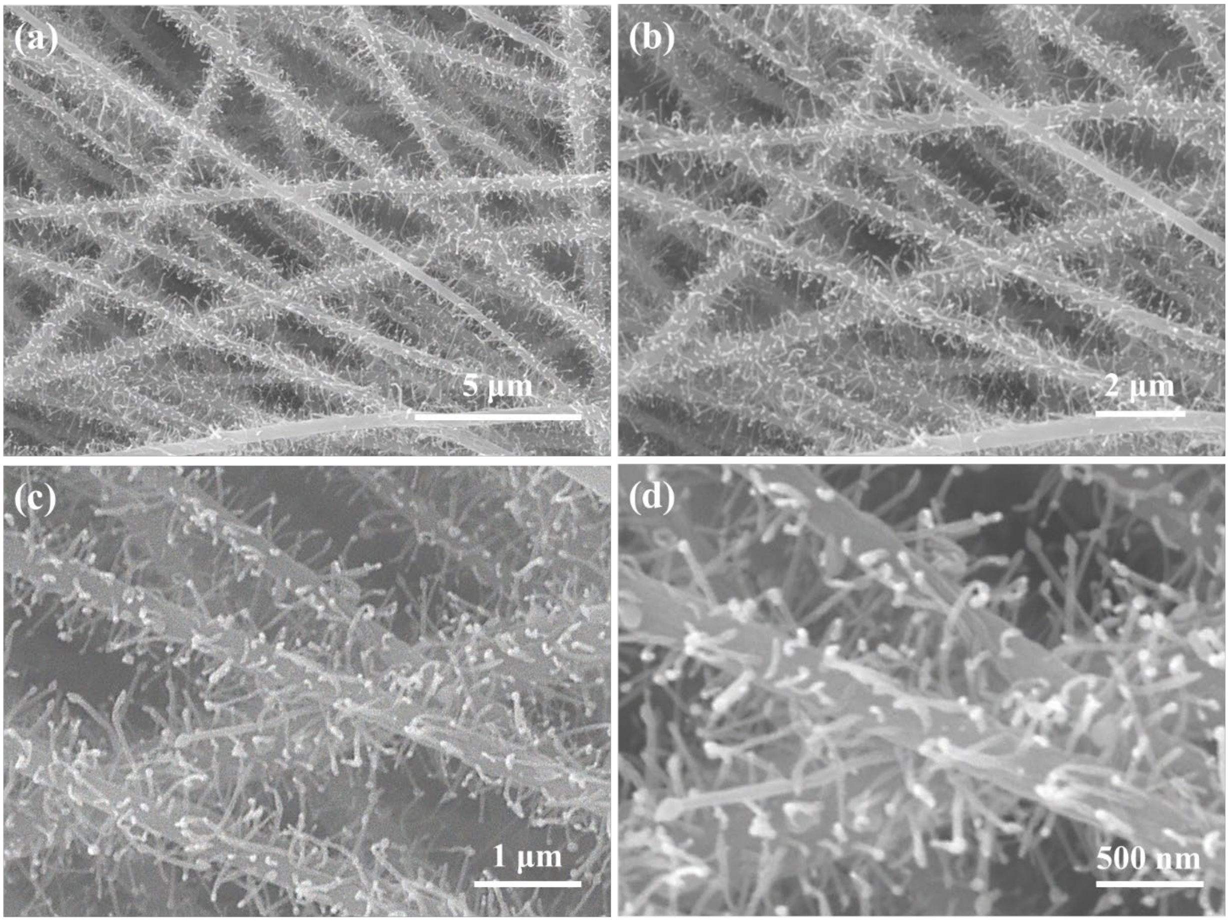

Fig. 2. Surface morphology of the FeNi-Co@CM electrode observed by SEM.

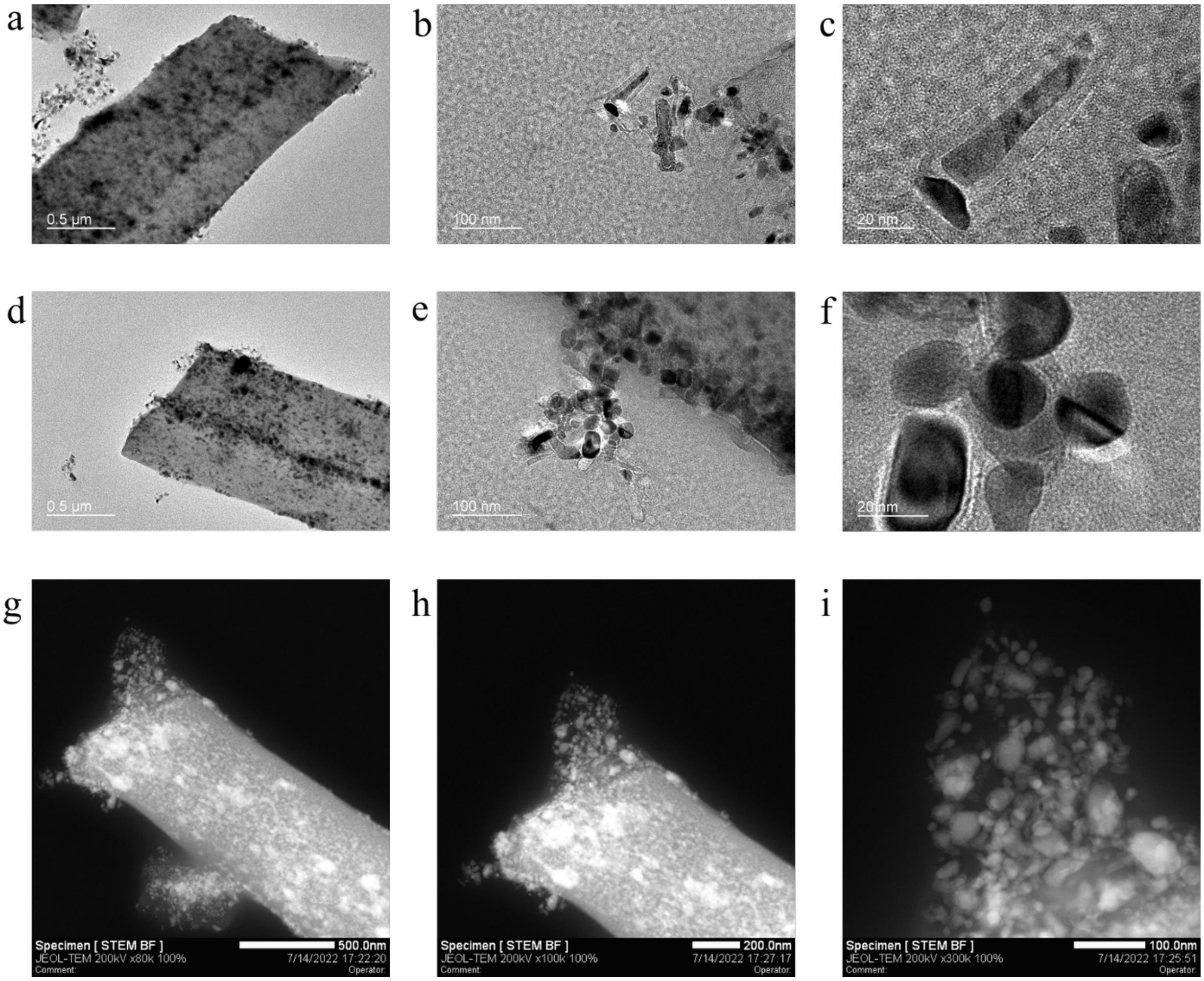

Fig. 3. (a-f) High-resolution TEM images of FeNi-Co@CM electrode. (g-i) High-angle annular dark-field (HAADF-STEM) images of FeNi-Co@CM electrode.

To further investigate the fine structure of the catalyst, TEM was applied to characterize the FeNi-Co@CM electrode (Fig. 3). Firstly, it can be seen that there are metal nanoparticles distributed on the surface of the carbon fibers. However, the number of carbon hairs grown on the surface of carbon fibers characterized by TEM is small and differs from the SEM characterization results. The main reason is that during the TEM characterization process, the electrodes are ground to obtain the catalyst powder and the dispersant alcohol is added for sonication. This process resulted in a large number of in situ self-grown carbon hairs coming off the surface of the carbon fiber. By finely characterizing the carbon hairs remaining on the surface of the carbon fibers, the presence of fine rod-shaped (Fig. 3b-c) or elliptical (Fig. 3e-f) metal nanoparticles with a diameter of approximately 10 to 20 nm can be observed in the carbon hairs. These properties of FeNi-Co@CM electrodes can be further verified by HAADF-STEM images (Fig. 3g-i), where metal nanoparticles can be found in carbon fibers and carbon hairs.

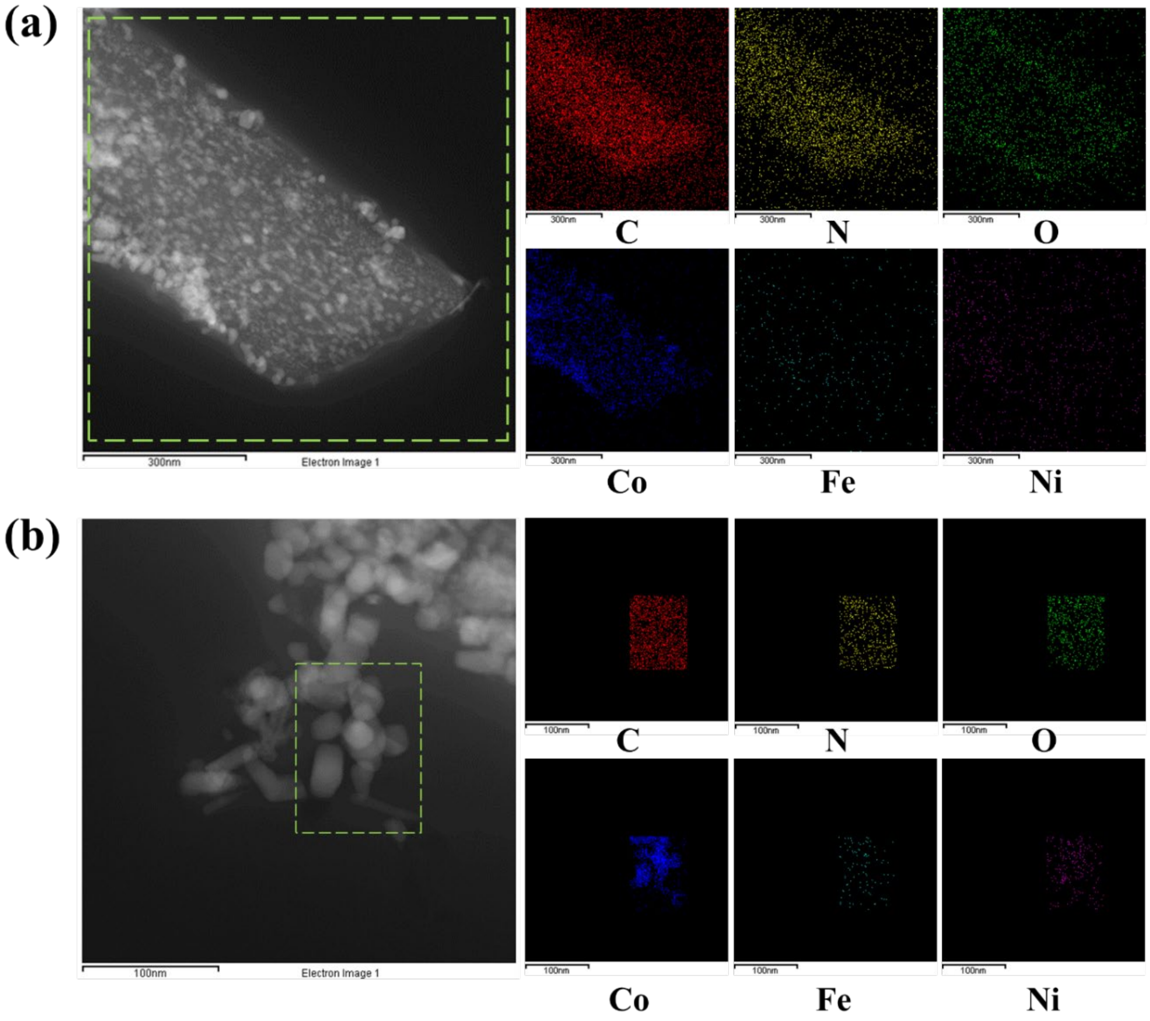

Fig. 4. STEM images for elemental mapping by energy-dispersive spectroscopy of FeNi-Co@CM electrode.

In addition, energy dispersive X-ray spectroscopy (EDS) analysis was performed to reveal the distribution of elements on the surface of the carbon fibers and carbon hairs. The STEM image in Fig. 4a demonstrates the distribution of elements on the carbon fibers inside the electrode. It can be seen that the main non-metallic elements on the carbon fiber include carbon, nitrogen and oxygen, all of which are uniformly present on the carbon fiber, while the portion with the highest content of carbon is highlighted in red in Fig. 4. Furthermore, according to STEM images for metal element mapping, the white spots on the carbon fibers in the HAADF-STEM images are mainly cobalt-associated nanoparticles. The elemental STEM images of Fe and Ni are almost absent, which can be attributed to the low content of Fe and Ni in the whole electrode (<0.1%, Fig. S3 and Table S1). According to the result determined by an inductively coupled plasma mass spectrometry (ICP-MS), the atomic ratio of the three transition metal elements Co, Fe, and Ni of the FeNi-Co@CM electrode is 145:1:0.2 (Table S2). Fig. 4b shows the distribution of elements on carbon hairs attached to the surface of carbon fibers, and it can be seen that the distribution of elements on carbon hairs is similar to that of carbon fibers. This can confirm that the fine particles comprising the carbon hairs characterized by HRTEM are composed of cobalt-associated nanoparticles and their amorphous carbon encapsulating these particles.

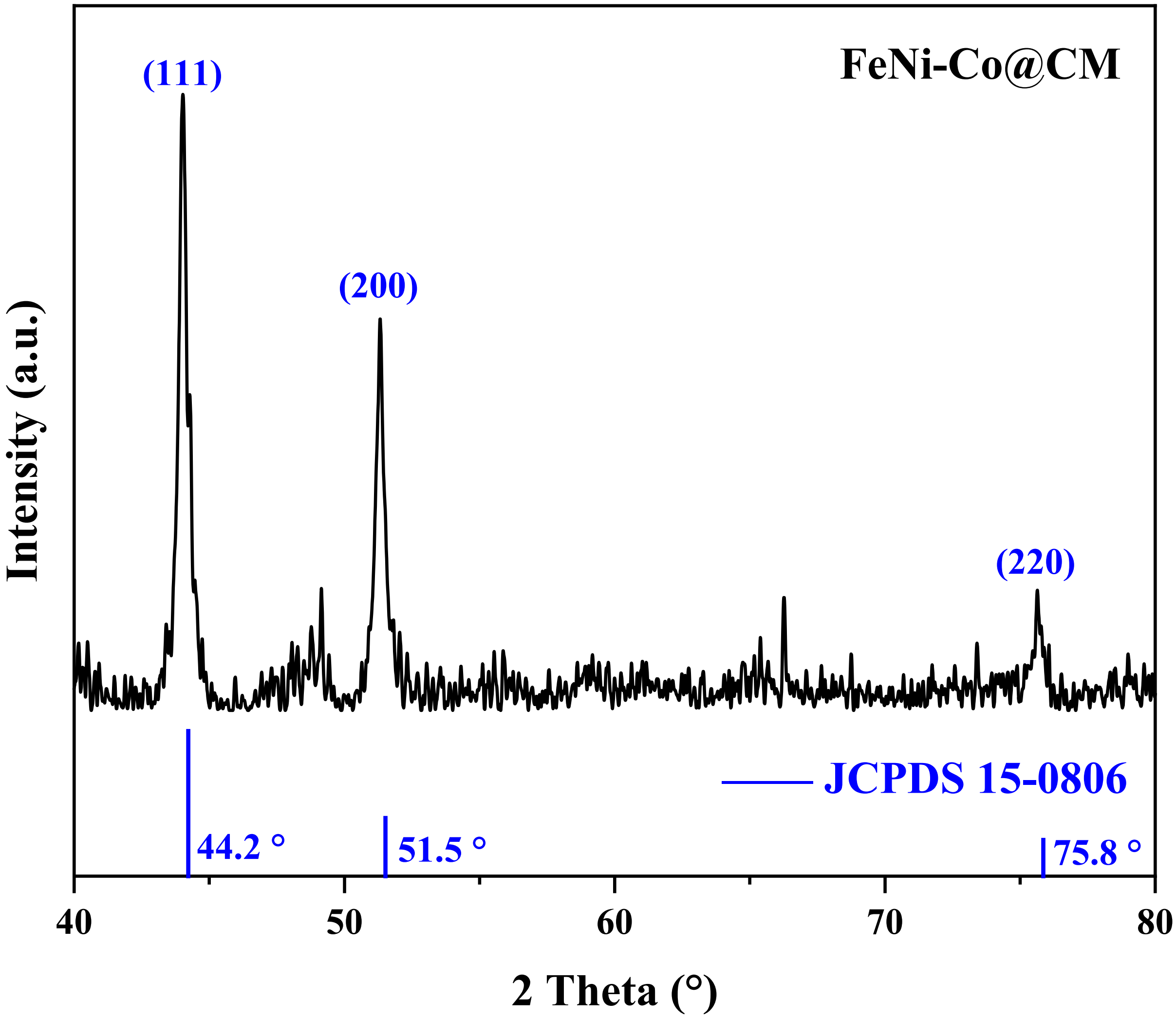

Fig. 5. XRD patterns of FeNi-Co@CM electrode.

To investigate the physical phase of the FeNi-Co@CM electrode material, XRD tests were carried out. The XRD diffraction pattern of the FeNi-Co@CM electrode is shown in Fig. 5. By comparing with the standard PDF card, it can be confirmed that the main phases of the FeNi-Co@CM electrode material is Co (PDF#15-0806) [33]. The diffraction peaks Co is assigned to the (111), (200) and (220) planes at 44.2°, 51.5°, and 75.8° respectively. A noteworthy point is that no peaks of Fe and Ni and their associated compounds were found on the XRD diffraction pattern, which can be attributed to the ultra-low content (less than 0.1%) of Fe and Ni.

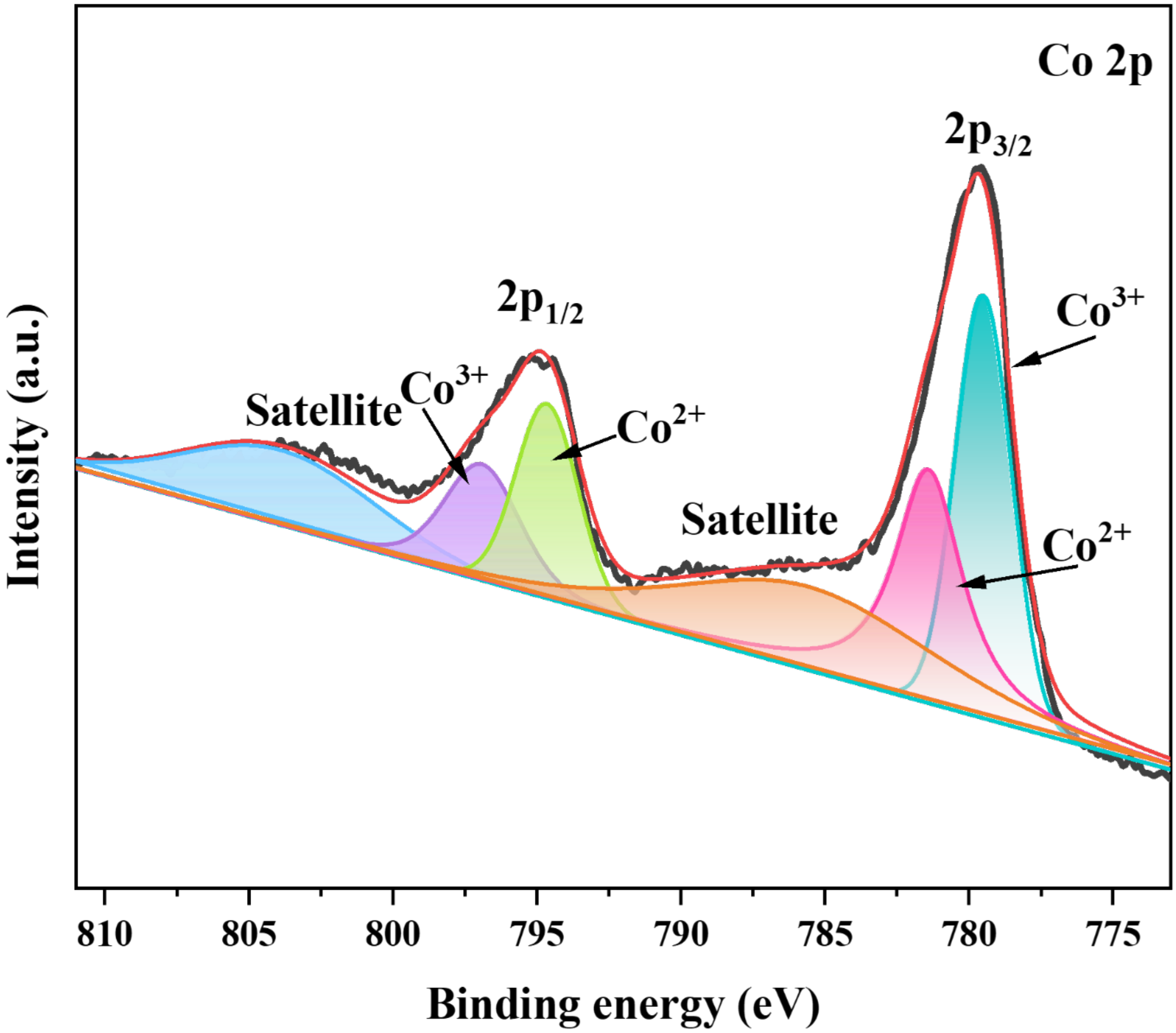

Fig. 6. XPS spectra of the Co 2p of the FeNi-Co@CM electrode.

To further explore the chemical and electronic state of the atoms within the FeNi-Co@CM electrode, the XPS test was carried out. The full-scan XPS spectra of FeNi-Co@CM electrode is shown in Fig. S4. Because the main component of the metal nanoparticles in the FeNi-Co@CM electrode is Co, while Fe and Ni are presented in the electrode as elemental dopants, therefore, the XPS spectra of Co, Fe and Ni are different. The XPS spectrum of Co 2p is shown in Fig. 6, where it is deconvoluted into two spin-orbiting double peaks for Co^{2+} and Co^{3+} and two satellite peaks. The two main peaks are located at 779.68 and 795.18 eV, corresponding to Co 2p3/2 and Co 2p1/2, where the spin-orbit splitting of the two peaks is about 15 eV [34]. Detailed deconvolution results show that FeNi-Co@CM electrode contains two Co species, identifiable as Co^{2+} (corresponding to the 780.45 eV peak in Co $2p_{3/2}$ and the 795.0 eV peak in Co $2p_{1/2}$) and Co^{3+} (corresponding to the 779.6 eV peak in Co $2p_{3/2}$ and the 796.5 eV peak in Co $2p_{1/2}$). The presence of Co^{2+} and Co^{3+} on the surface of the electrode can be attributed to the following two reasons: (1) During the preparation of the material, the metal oxide will not be completely reduced. (2) The oxidation of Co on the electrode surface in air, forming cobalt oxides such as CoO and Co_3O_4. In additional, it is worth noting that although Fe and Ni species are detected in the XPS full spectrum (Fig. S4), their low content results in low intensities in the XPS spectra and thus does not provide reliable information on the valence of the elements and is therefore omitted.

3.2 Electrochemical measurement results

For the purpose of providing a more informed interpretation of the experimental results, the reaction mechanism for the electrochemical synthesis of ammonia and the corresponding reaction equations are first presented here. The three-electrode electrochemical cell applied in this study is H-type cell, which consists of two important circuits. The first circuit, consists of a reference electrode and a working electrode, is primarily used for measuring the potential of the electrochemical reaction on the working electrode. The second or alternative circuit, made up of a working electrode and a counter electrode, transmits electrons to form a current flow to drive electrochemical reactions. In the electrochemical synthesis of ammonia, $N_2(g)$ enters the cathode chamber through a gas pipeline and dissolves in the electrolyte as $N_2(d)$ in the solution, and then migrates to the working electrode. On the working electrode, $N_2(d)$ electrochemically reacts with electrons and water molecules under the promotion of catalysts to generate ammonia and hydroxide ions, which can be described by the following reaction [35]:

$$N_2 + 8H_2O + 6e^- \rightarrow 2NH_3\cdot H_2O + 6OH^- \quad E_c^0 = -0.77 \text{ V vs. SHE} \tag{2}$$

Meanwhile, the hydroxide ions are driven by the electric field through the anion exchange membrane from the cathode compartment to the anode compartment. On the counter electrode, the hydroxide ions are oxidized, releasing electrons, and generating oxygen and water, expressed as follows [36]:

$$6OH^- \rightarrow 3H_2O + 6e^- + 3/2O_2 \quad E_a^0 = +0.4 \text{ V vs. SHE} \tag{3}$$

In the above-mentioned electrochemical ammonia synthesis process based on a three-electrode system, there are two important mass/charge transfer processes that need to be highlighted. The first is that electrons move from the anode to the cathode through an external circuit to form an electronic flow, and the second is that the hydroxide ions pass through the anion exchange membrane from the cathode to the anode to form an ionic flow. Macroscopically, a circuit is formed by the electronic flow and ionic flow. In summary, the overall reaction in alkaline aqueous media can be expressed as follows:

$$N_2 + 5H_2O \rightarrow 2NH_3 \cdot H_2O + 3/2O_2 \quad E^0 = 1.17\ V \tag{4}$$

To determine the potential window of electrochemical synthesis of ammonia for the FeNi-Co@CM electrode, potentials ranging from 0 to -0.35 V vs. RHE were tested for 600 s to ascertain that the electrode has reached an activated state [31]. The polarization curves were thereafter obtained by using the data collected from the final 100 s. The results of the LSV test are shown in Fig. 7.

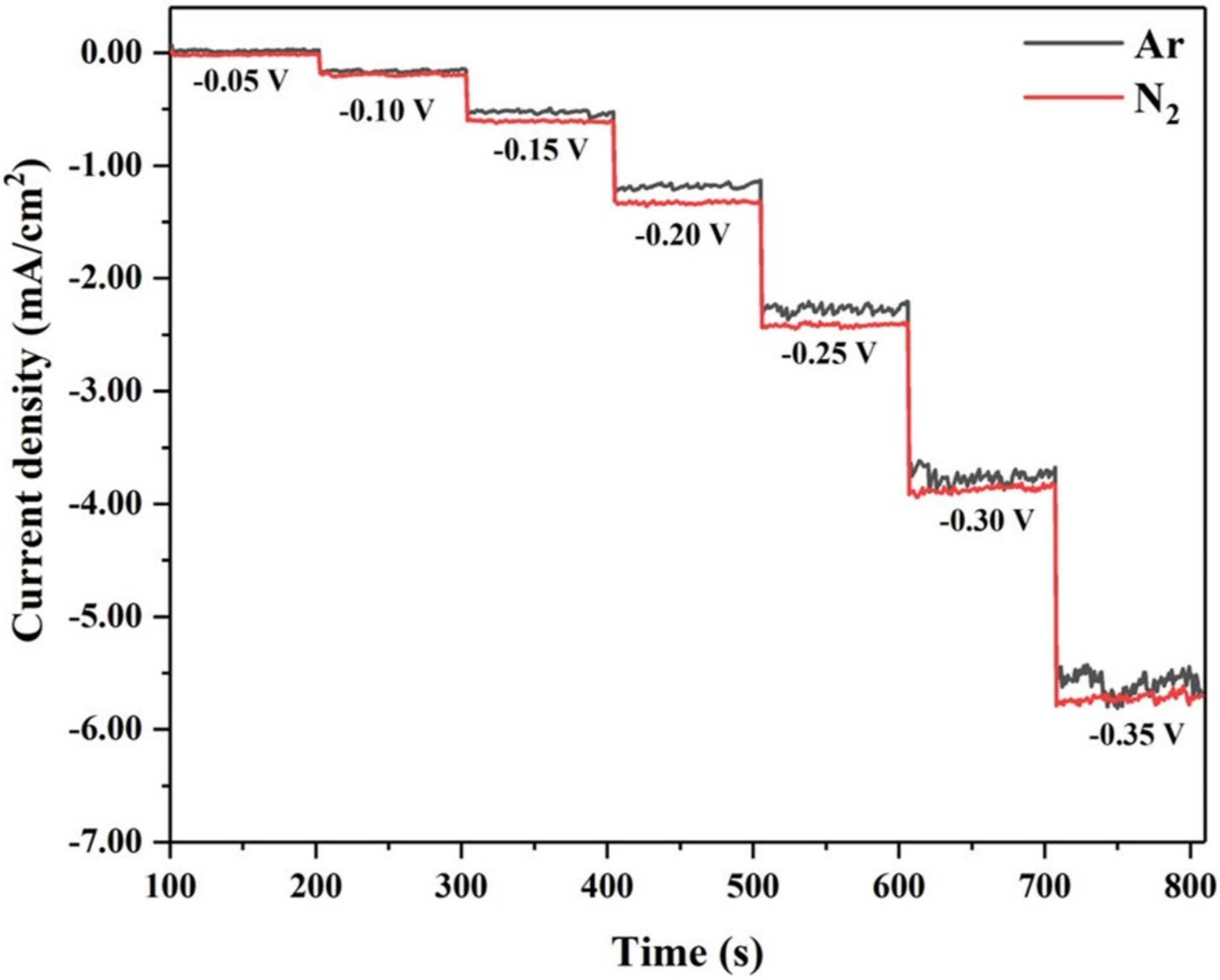

Fig. 7. The current density gap between N_2 and Ar bubbling NRR at various potentials (-0.05 V to -0.35 V vs. RHE).

It can be seen that the current density gap between Ar bubbling and N_2 bubbling increases first and then decreases with an applied potential ranging from -0.05 to -0.35 V vs. RHE, which reached the peak value at -0.20 V vs. RHE. Therefore, the obtained results suggest that the potential windows around -0.15 to -0.25 V vs. RHE has a higher possibility in which NRR can occur with the use of the FeNi-Co@CM electrode. After obtaining the optimal potential window for NRR, the chronoamperometry was conducted at different potentials (-0.05 to -0.35 V vs. RHE) for 2.0 h. The I-t curves at various potentials are presented in Fig. S5. To measure the yield of ammonia, the electrolyte in the cathode chamber is collected after the electrochemical reaction. The collected solutions are then mixed with a color reagent for UV-Vis absorption at a wavelength of 650 nm. The ammonia concentration can be calculated based on the absolute calibration curve for standard NH_4Cl solutions. Once the concentration of the produced ammonia is determined, the ammonia yield rate, r $[NH_3]$, can be obtained by the following equation [28]:

$$r\,[NH_3] = (C_{NH_3}\ x\ V)/(t \text{ x } m_{cat}) \tag{5}$$

Here, C_{NH_3} (μg/mL) is the NH_3 concentration after electrolysis, V (mL) is the volume of the electrolyte in the cathode chamber, t (h) is the reaction time for electrochemical synthesis of ammonia, and m (mg) is the mass loading of the catalysts. Therefore, the unit of $r[NH_3]$ in this study is μg h^{-1} mg^{-1}. Furthermore, the FE for ammonia production can be calculated by the following equation:

$$FE = (3F\ x\ C_{NH_3}\ x\ V)\ x100\%/Q \tag{6}$$

Here, F is the Faraday constant and Q is the quantity of the applied electricity. The ammonia yield rates and FE at various potentials are shown in Fig. 8.

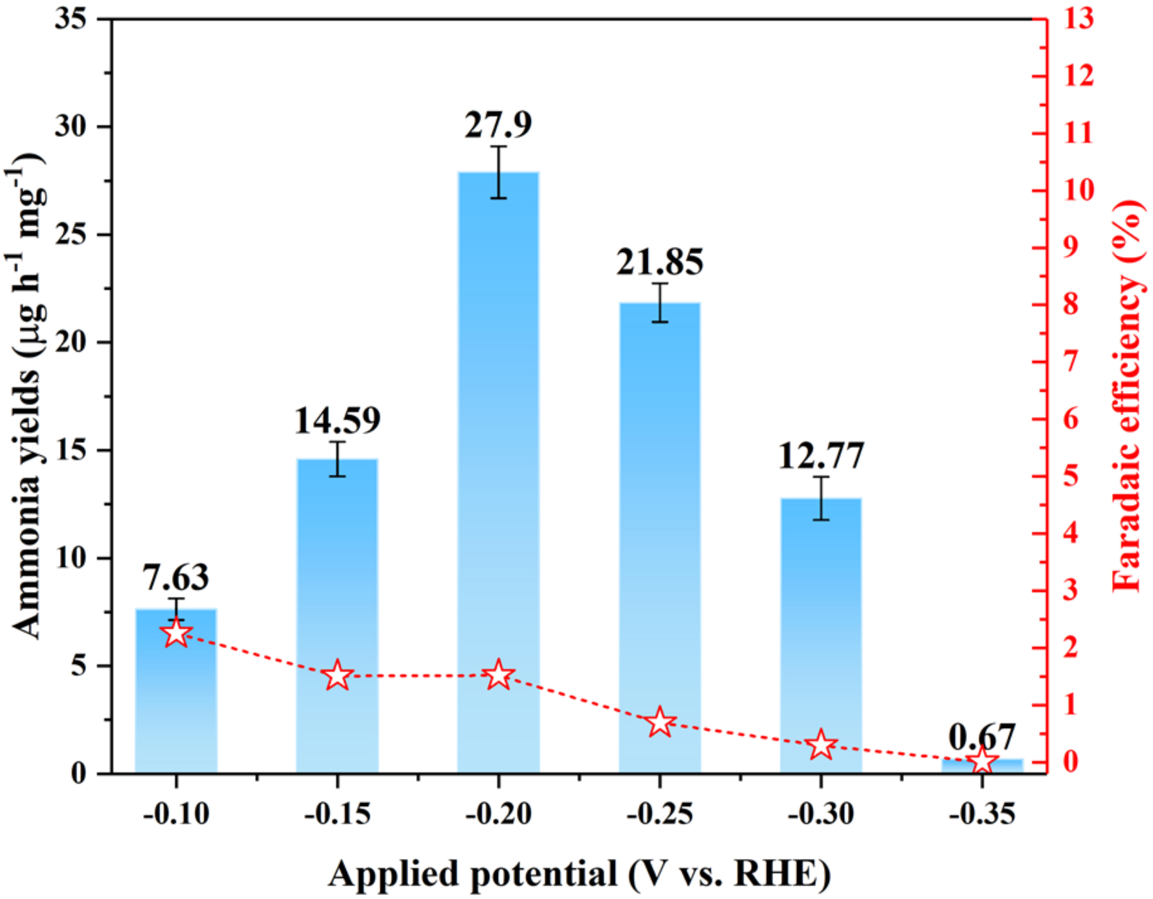

Fig. 8. The ammonia yields and Faradaic efficiency at various potentials.

It can be seen that ammonia yields increase as the applied potential increases from -0.1 to -0.2 V vs. RHE. The highest ammonia yields of 27.9 μg h^{-1} mg^{-1} is achieved at the potential of -0.2 V vs. RHE, which is higher than most of the recently reported works where iron-group-based electrocatalysts were employed (refer to Fig. 9 and Table 1). However, when the applied potential exceeds -0.25 V vs. RHE, the NRR performance of the FeNi-Co@CM electrode is dramatically reduced, which is attributed to the more active HER process at high potential, producing more hydrogen on the surface of the catalyst and thus hindering the effective adsorption of N_2 on the catalyst surface. Fig. 8 further reveals that the FE decreases with higher applied potentials. The possible reason for this phenomenon is that the current density corresponding to the lower potential was relatively small (See Fig. S5), therefore the FE calculated according to Eq. 6 is higher.

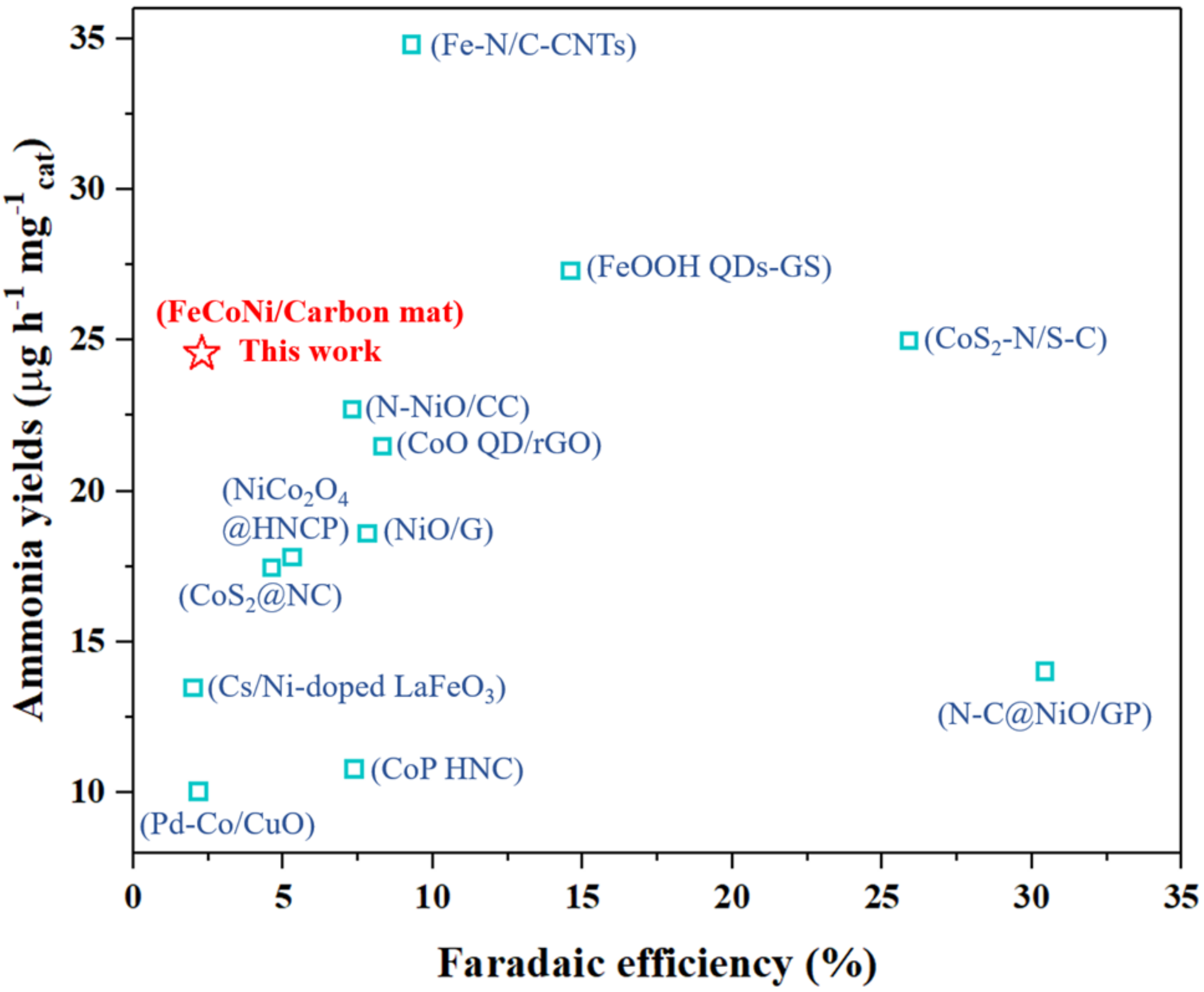

Fig. 9. The comparable results of our work and other recently reported iron-group electrocatalysts for ambient ammonia synthesis.

Table 1 Comparison of our results with other recently reported studies that used iron-group electrocatalysts for ambient ammonia synthesis.

Catalytic materials	Ammonia yields ($\mu g \cdot h^{-1} \cdot mg^{-1}_{cat}$)	Faradaic efficiency (%)	Applied potential (VS. RHE)	Electrolyte	References
CoO QD/rGO	21.5	8.3	−0.6 V	0.1 M Na_2SO_4	[22]
CoS_2-N/S-C	25	25.9	−0.05 V	0.05 M H_2SO_4	[37]
CoS_2@NC	17.45	4.6	−0.15 V	0.1 M HCl	[23]
CoP HNC	10.78	7.36	−0.4 V	1.0 M KOH	[38]
$NiCo_2O_4$@HNCP	17.8	5.3	−0.25 V	0.1 M Na_2SO_4	[39]
Pd-Co/CuO	10.04	2.16	−0.2 V	0.1 M KOH	[40]
Cs/Ni-doped $LaFeO_3$	13.46	1.99	2 V	2.0 M KOH	[41]
Fe-N/C-CNTs	34.83	9.28	−0.2 V	0.1 M KOH	[42]
NiO/G	18.6	7.8	−0.7 V	0.1 M Na_2SO_4	[43]
N-NiO/CC	22.7	7.3	−0.5 V	0.1 M $LiClO_4$	[44]
N-C@NiO/GP	14.022	30.43	−0.2 V	0.1 M HCl	[45]
FeOOH QDs-GS	27.3	14.6	−0.4	0.1 M $LiClO_4$	[46]
FeNi-Co@CM	27.9	1.52	−0.2 V	1.0 M KOH	This work

The FeNi-Co@CM stability test result is shown in Fig. 10. It can be seen that the ammonia yield rate and the FE of the developed electrode can be maintained at a high level for ten cycles. These properties indicate that the FeNi-Co@CM electrode exhibits good stability for electrocatalytic nitrogen reduction to ammonia under ambient conditions. The SEM results of the FeNi-Co@CM electrode before and after the stability test reveal the reason for the decrease in electrocatalytic nitrogen reduction performance of the electrode, as shown in Fig. S6. It can be seen that the number of carbon hairs on the surface of carbon fiber has been reduced, thereby reducing the number of metal nanoparticles (mainly Co) on the electrode. This change in microstructure reduces the number of catalysts on the electrode surface, resulting in fewer active sites for electrochemical reactions and thus a reduction in NRR performance. The carbon hairs coming off the surface of the carbon fiber can be attributed to the following reasons: (1) During the experiment, the electrolyte on the cathode side was constantly stirred with a magnetic stirrer, which may have accelerated the shedding of carbon hairs from the surface of the carbon fiber. (2) The low solubility of nitrogen gas during the experiments means that the bubbles, which are poured into the cathode chamber, are constantly hitting the electrode which may also accelerate the removal of carbon hairs over time.

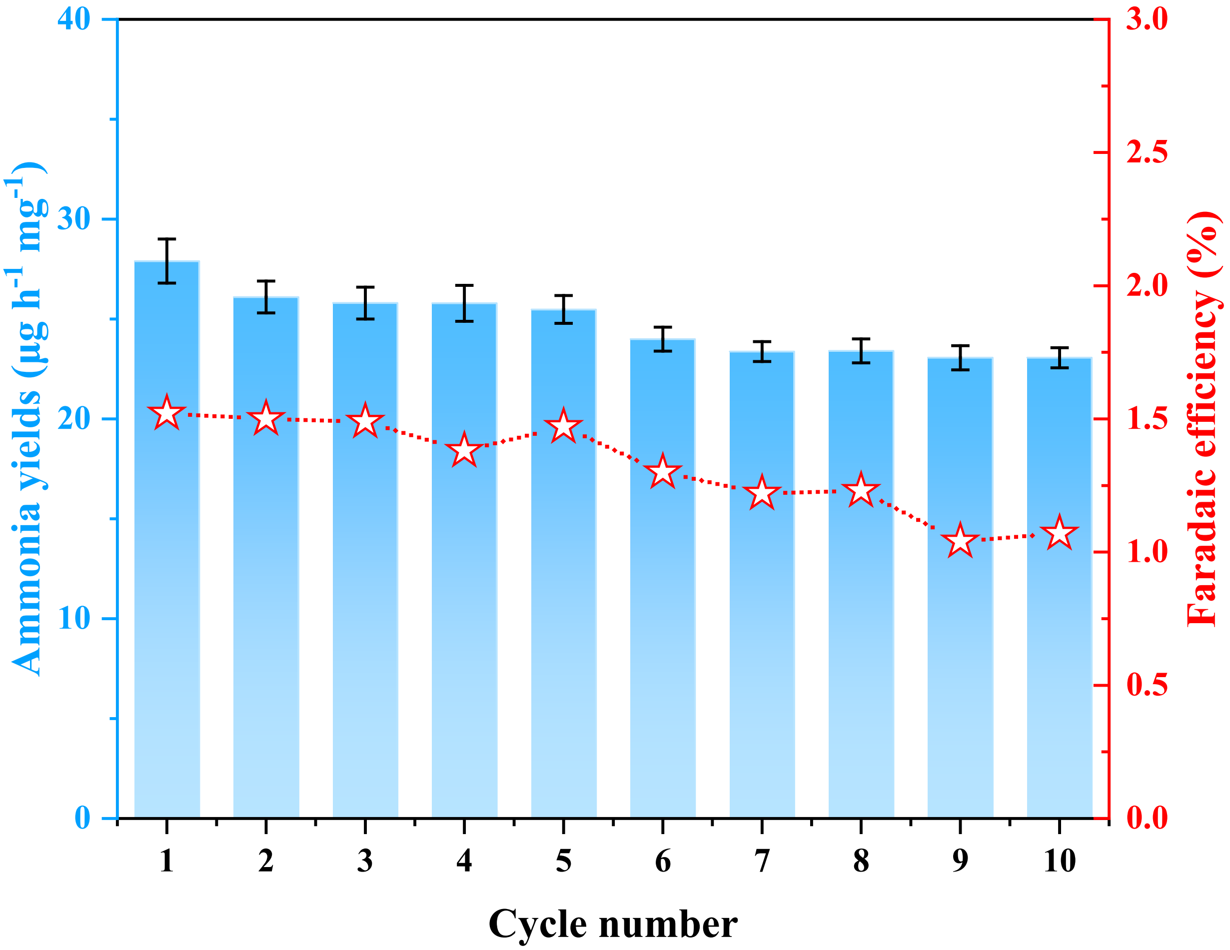

Fig. 10. FeNi-Co@CM electrode stability test results.

To confirm that the detected ammonia is a product of electrochemical ammonia synthesis rather than contaminants, two comparative experiments were conducted. As shown in Fig. S7, the results reveal that there is no absorption peak under Ar bubbling conditions with the same applied potential, indicating that the detected ammonia is produced by the electrochemical NRR rather than any other ammonia contaminations during the cell operations as well as the N-precursor introduced during the material preparation. This can be further explained by the detection results of open-circuit conditions (Fig. S8) in which no absorption peak of ammonia was observed. In addition, hydrazine is also considered as a possible product. However, in this study, hydrazine will not be produced under the applied potentials in terms of the thermodynamics perspective. Experimental results also confirm that there is no hydrazine production during the electrochemical NRR process (Fig. S9).

3.3 Discussion

In this section, the working mechanism of the electrocatalytic NRR based on FeNi-Co@CM will be first discussed from different scale, including the electrode scale, the catalyst scale, and the atomic scale, as shown in Fig. 11.

Firstly, at the electrode scale (Fig. 11-a), gaseous nitrogen N_2(g) is passed through the gas-liquid interface (g/l interface) into the electrolyte, after which a small amount of nitrogen is dissolved in the electrolyte, named N_2(d). The N_2(d) then migrates from the electrolyte to the surface of the electrode, where it undergoes an NRR to produce ammonia, driven by the potential applied by the external circuit. The unreacted nitrogen gas, on the other hand, escapes from the electrolyte side across the gas-liquid interface.

Secondly, at the catalyst scale, two main interfaces are included, the first being the g/l interface and the second being the liquid/solid interface (l/s interface-red dashed line in Fig. 11-b). The detailed reaction process is described as follows: the N_2(d) adsorbs on the surface of the cobalt-based catalyst nanoparticles and combines with electrons and water molecules at the l/s interface to produce $NH_3 \cdot H_2O$ (the form of ammonia produced exists in the alkaline electrolyte) and OH^-. In this case, the electrons come from an external circuit and are conducted through the carbon support to the catalyst nanoparticles and then from the catalyst nanoparticles to the l/s interface. The water molecules in the electrolyte here take on the role of providing the proton, as the electrolyte is alkaline and cannot provide a direct source of protons. In addition, the competing HER of NRR can be seen in Fig. 11-b, which also occurs at the solid/liquid interface and competes for electrons with the NRR.

Thirdly, the atomic scale focuses on describing how nitrogen molecules are transformed step by step into ammonia. In general, the mechanism of NRR at the atomic scale is divided into two pathways, namely the associative and dissociative pathways [47,48]. For the dissociative pathway, the nitrogen-nitrogen triple bond in the nitrogen molecule is first completely broken and the nitrogen molecule is divided into two nitrogen atoms (N), which then adsorb to the catalyst surface and are gradually protonated to produce ammonia molecules, which are then desorbed from the catalyst surface. For the associative pathway, on the other hand, the nitrogen-nitrogen triple bond in the nitrogen molecule is incompletely broken. The nitrogen molecule first adsorbs to the surface of the catalyst, after which the nitrogen-nitrogen triple bond breaks to become a nitrogen-nitrogen double bond, which is then progressively protonated. In accordance with the previously published works on electrochemical ammonia synthesis using similar materials and electrolytes [49–51], we believe that the reaction mechanism of electrochemical ammonia synthesis in this work follows an associative pathway, as shown in Fig. 11-c.

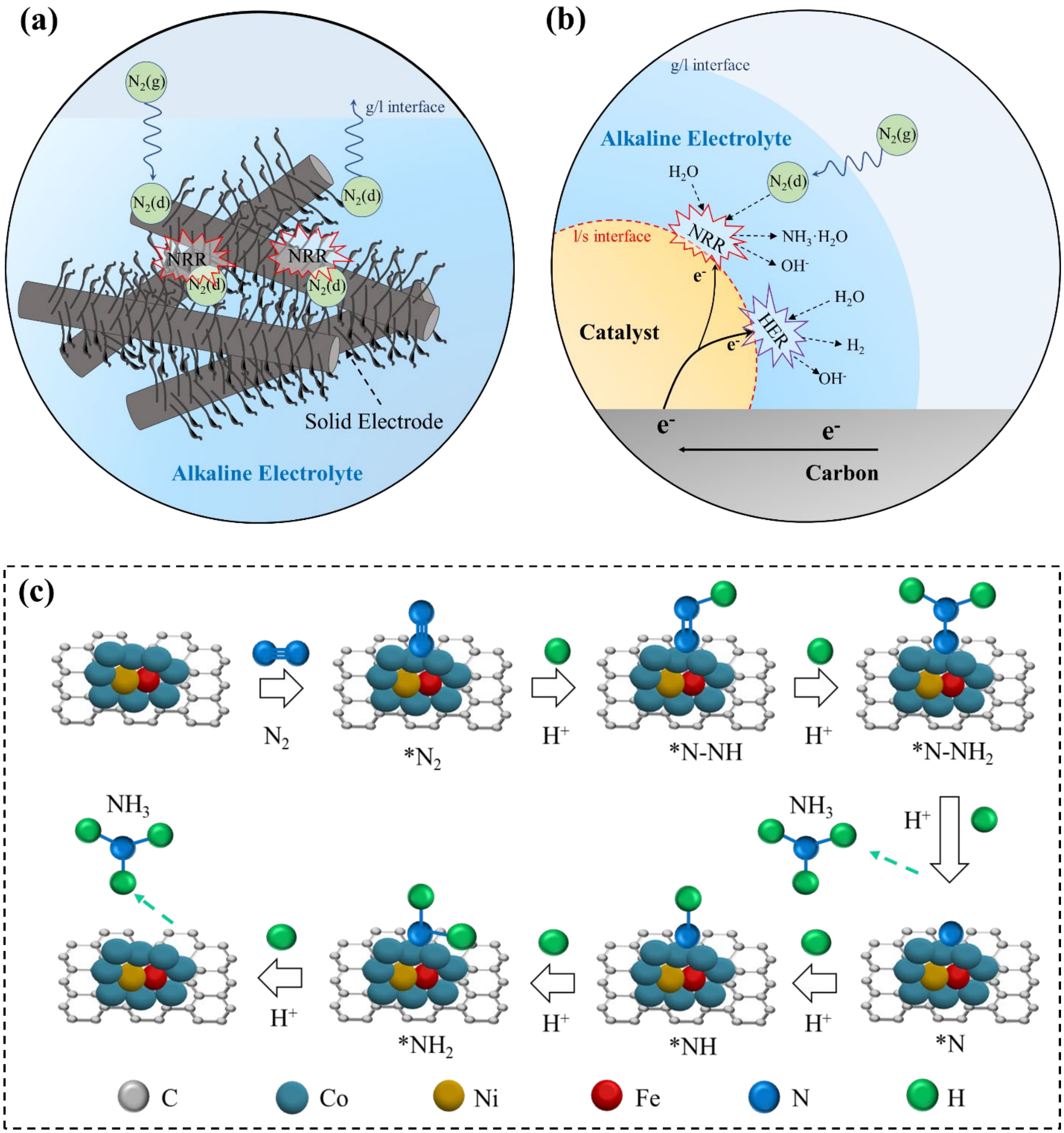

Fig. 11. Proposed working mechanism of electrocatalytic NRR based on FeNi-Co@CM electrode. (a) Electrode-scale view. (b) Catalyst-scale view. (c) Atomic-scale view.

The nitrogen molecule is first adsorbed on the surface of the cobalt-based catalyst nanoparticles ($*N_2$), followed by incomplete breaking of N≡N into a N=N. Meanwhile, a proton (H^+) from the water molecule combines with a nitrogen atom away from the Co atom to form a N=N-H. After adding three protons, the nitrogen-nitrogen triple bond is completely broken, forming the first NH_3 which then desorbs from the catalyst surface. Similar to the first nitrogen atom, the second nitrogen atom is then progressively protonated, and finally, the ammonia molecule is formed and then desorbed. Thus, the NRR process is completed, and one nitrogen molecule produces two ammonia molecules. Previous studies have shown that for the transition metals Ru, Co, Ni, and Rh, the first charge and proton transfer process ($N_2 + H^+ + e^- = {}^*N_2H$) is the rate-determining step for the associative mechanism while the N_2 cleavage determines the activity of the metal surface [52,53]. In summary, the synthesized FeNi-Co@CM electrode in this study demonstrates a good electrochemical NRR performance, achieving an ammonia yield rate of 27.9 μg h^{-1} mg^{-1} and a FE of 1.52 %. The high ammonia yields exhibited by the FeNi-Co@CM electrode can be ascribed to the following reasons: (1) The major catalyst material used in this study is Co, which possesses an electronic configuration of $3d^7 4s^2$, and therefore easier to accept the electron density from N_2. In addition, cobalt-based catalysts can donate electrons to the π^* orbital of N≡N, thereby enhancing N_2 adsorption and weakening the N≡N bond [54]. (2) The unique structure of the electrode, with carbon hairs attached to the surface of the carbon fiber, can significantly increase the specific surface area of the electrode surface, as demonstrated in previous work [32]. The specific surface area of the electrode with carbon hairs on the carbon fiber (282.8 m^2/g) is much higher than that of the electrode without carbon hairs on the carbon fiber (181.1 m^2/g). (3) FeNi-doped cobalt electrodes have stronger electron conductivity than pure cobalt electrodes, as shown by the results in Fig. S10.

4. Concluding remarks

In this study, a self-supporting carbon mat with FeNi-doped Co catalysts ($Co_{145}Fe_1Ni_{0.2}$) fabricated by electrospinning was used as an electrode for electrochemical ammonia synthesis. To evaluate the electrochemical ammonia synthesis performance of FeNi-Co@CM electrode, a three-electrode electrochemical cell has been constructed using the FeNi-Co@CM as working electrode, a platinum mesh as counter electrode, and a Ag/AgCl electrode as reference electrode. An ammonia yield rate of 27.9 $\mu g\ h^{-1}\ mg^{-1}$ and a Faradaic efficiency of 1.52 % in 1.0 M KOH are achieved from the experimental investigation. The control experiments indicated that the ammonia detected in the experiments originated from the nitrogen reduction reaction rather than contaminants in the reaction environment. In addition, the FeNi-Co@CM electrode can maintain a high level of ammonia production for more than ten cycles. The result analysis shows that the performance degradation of the electrode can be attributed to the microscopic change of the electrode structure, that is, the shedding of the carbon hairs on the surface of the carbon fibers. Based on the electrochemical ammonia synthesis performance demonstrated by the FeNi-Co@CM electrode, the working mechanism of the nitrogen reduction reaction is explored at three different scales: electrode scale, catalyst scale, and atomic scale. These analyses, including mass transport (transport of speciess, ions and electrons), reaction interfaces and reaction intermediates, provide a comprehensive understanding of nitrogen reduction reactions. Our study therefore provides insights and also paves the way for the application of FeNi-doped cobalt-based catalysts to promote the electrochemical conversion of nitrogen to ammonia under ambient conditions.

Acknowledgements

The work described in this paper was supported by a grant from the Research Grants Council of the Hong Kong Special Administrative Region, China (No. N_PolyU559/21) and a grant from the Shenzhen Science and Technology Innovation Commission (No. JCYJ20210324131406018).

References

[1] M.J. Palys, H. Wang, Q. Zhang, P. Daoutidis, Renewable ammonia for sustainable energy and agriculture: vision and systems engineering opportunities, Curr. Opin. Chem. Eng. 31 (2021) 100667. https://doi.org/10.1016/j.coche.2020.100667.

[2] M. Zhang, H. Li, X. Duan, P. Zou, G. Jeerh, B. Sun, S. Chen, J. Humphreys, M. Walker, K. Xie, S. Tao, An efficient symmetric electrolyzer based on bifunctional perovskite catalyst for ammonia electrolysis, Adv. Sci. 8 (2021) 14–17. https://doi.org/10.1002/advs.202101299.

[3] Y. Guo, Z. Pan, L. An, Carbon-free sustainable energy technology: Direct ammonia fuel cells, J. Power Sources. 476 (2020) 228454. https://doi.org/10.1016/j.jpowsour.2020.228454.

[4] N. Morlanés, S.P. Katikaneni, S.N. Paglieri, A. Harale, B. Solami, S.M. Sarathy, J. Gascon, A technological roadmap to the ammonia energy economy: Current state and missing technologies, Chem. Eng. J. 408 (2021). https://doi.org/10.1016/j.cej.2020.127310.

[5] X. Zhu, S. Mou, Q. Peng, Q. Liu, Y. Luo, G. Chen, S. Gao, X. Sun, Aqueous electrocatalytic N2 reduction for ambient NH3 synthesis: Recent advances in catalyst development and performance improvement, J. Mater. Chem. A. 8 (2020) 1545–1556. https://doi.org/10.1039/c9ta13044f.

[6] G. Li, Z. Pan, H. Lin, L. An, In-situ formation of bismuth nanoparticles on nickel foam for ambient ammonia synthesis via electrocatalytic nitrogen reduction, J. Alloys Compd. 875 (2021) 160006. https://doi.org/10.1016/j.jallcom.2021.160006.

[7] M. Wang, S. Liu, H. Ji, T. Yang, T. Qian, C. Yan, Salting-out effect promoting highly efficient ambient ammonia synthesis, Nat. Commun. 12 (2021). https://doi.org/10.1038/s41467-021-23360-0.

[8] H. Shen, C. Choi, J. Masa, X. Li, J. Qiu, Y. Jung, Z. Sun, Electrochemical ammonia synthesis: Mechanistic understanding and catalyst design, Chem. 7 (2021) 1708–1754. https://doi.org/10.1016/j.chempr.2021.01.009.

[9] C. Lee, Q. Yan, Electrochemical reduction of nitrogen to ammonia: Progress, challenges and future outlook, Curr. Opin. Electrochem. 29 (2021) 100808. https://doi.org/10.1016/j.coelec.2021.100808.

[10] T. Li, Y. Wu, M. Pei, Screening of transition metal single-atom catalysts doped on γ-graphyne-like BN sheet for efficient nitrogen reduction reaction, J. Alloys Compd. 908 (2022) 164675. https://doi.org/10.1016/j.jallcom.2022.164675.

[11] C. Smith, L. Torrente-Murciano, Guidance for targeted development of ammonia synthesis catalysts from a holistic process approach, Chem Catal. 1 (2021) 1163–1172. https://doi.org/10.1016/j.checat.2021.09.015.

[12] J. Li, F. Wei, C. Dong, Z. Wang, Z. Xiu, X. Han, Recent progress of inorganic metal-based catalysts in electrocatalytic synthesis of ammonia, Mater. Today Energy. 21 (2021). https://doi.org/10.1016/j.mtener.2021.100766.

[13] Y. Zhou, C.Q. Xu, Z. Tan, H. Cai, X. Wang, J. Li, L. Zheng, C.T. Au, J. Li, L. Jiang, Integrating dissociative and associative routes for efficient ammonia synthesis over a TiCN-promoted Ru-based catalyst, ACS Catal. 12 (2022) 2651–2660. https://doi.org/10.1021/acscatal.1c05613.

[14] M. Nazemi, S.R. Panikkanvalappil, M.A. El-Sayed, Enhancing the rate of electrochemical nitrogen reduction reaction for ammonia synthesis under ambient conditions using hollow gold nanocages, Nano Energy. 49 (2018) 316–323. https://doi.org/10.1016/j.nanoen.2018.04.039.

[15] S. Chung, D.H. Seo, M. Choi, X. Mao, A. Du, K. Ham, S. Giddey, J. Lee, H.K. Ju, Rhodium-molybdenum oxide electrocatalyst with dual active sites for electrochemical ammonia synthesis under neutral pH condition, J. Electroanal. Chem. 896 (2021) 115157. https://doi.org/10.1016/j.jelechem.2021.115157.

[16] X. Cai, F. Yang, L. An, C. Fu, L. Luo, S. Shen, J. Zhang, Evaluation of electrocatalytic activity of noble metal catalysts toward nitrogen reduction reaction in aqueous solutions under ambient conditions, ChemSusChem. 15 (2022) 22–25. https://doi.org/10.1002/cssc.202102234.

[17] P. Hou, Y. Huang, F. Ma, G. Zhu, J. Zhang, X. Wei, P. Du, J. Liu, Computational screening and catalytic origin of transition metal supported on g-t-C_3N_4 as single-atom catalysts for nitrogen reduction reaction, Appl. Surf. Sci. 599 (2022) 153880. https://doi.org/10.1016/j.apsusc.2022.153880.

[18] X. Chen, W.J. Ong, X. Zhao, P. Zhang, N. Li, Insights into electrochemical nitrogen reduction reaction mechanisms: Combined effect of single transition-metal and boron atom, J. Energy Chem. 58 (2021) 577–585. https://doi.org/10.1016/j.jechem.2020.10.043.

[19] L. Zhang, H. Shoushuang, J. Bao, L. Liu, T. Ye, X. Cong, K. Uvdal, Z. Hu, Intersperse copper nanoparticles into 3D fibrous silica-supported carbon spheres for electrocatalytic nitrogen reduction, J. Alloys Compd. 910 (2022) 164759. https://doi.org/10.1016/j.jallcom.2022.164759.

[20] Y. Luo, M. Li, Y. Dai, R. Zhao, F. Jiang, S. Wang, Y. Huang, Transition metal-modified Co_4 clusters supported on graphdiyne as an effective nitrogen reduction reaction electrocatalyst, Inorg. Chem. 60 (2021) 18251–18259. https://doi.org/10.1021/acs.inorgchem.1c02880.

[21] M. Zheng, H. Xu, Y. Li, K. Ding, Y. Zhang, C. Sun, W. Chen, W. Lin, Electrocatalytic nitrogen reduction by transition metal single-atom catalysts on polymeric carbon nitride, J. Phys. Chem. C. 125 (2021) 13880–13888. https://doi.org/10.1021/acs.jpcc.1c03425.

[22] K. Chu, Y.P. Liu, Y.B. Li, H. Zhang, Y. Tian, Efficient electrocatalytic N_2 reduction on CoO quantum dots, J. Mater. Chem. A. 7 (2019) 4389–4394. https://doi.org/10.1039/c9ta00016j.

[23] P. Wei, H. Xie, X. Zhu, R. Zhao, L. Ji, X. Tong, Y. Luo, G. Cui, Z. Wang, X. Sun, CoS_2 nanoparticles-embedded N-doped carbon nanobox derived from ZIF-67 for electrocatalytic N_2-to-NH_3 fixation under ambient conditions, ACS Sustain. Chem. Eng. 8 (2020) 29–33. https://doi.org/10.1021/acssuschemeng.9b06272.

[24] K. Chu, Y.H. Cheng, Q.Q. Li, Y.P. Liu, Y. Tian, Fe-doping induced morphological changes, oxygen vacancies and Ce^{3+}-Ce^{3+} pairs in CeO_2 for promoting electrocatalytic nitrogen fixation, J. Mater. Chem. A. 8 (2020) 5865–5873. https://doi.org/10.1039/c9ta14260f.

[25] Z. Wei, J. He, Y. Yang, Z. Xia, Y. Feng, J. Ma, Fe, V-co-doped C_2N for electrocatalytic N_2-to-NH_3 conversion, J. Energy Chem. 53 (2020) 303–308. https://doi.org/10.1016/j.jechem.2020.04.014.

[26] J.W. Zhang, H. Zhang, T.Z. Ren, Z.Y. Yuan, T.J. Bandosz, FeNi doped porous carbon as an efficient catalyst for oxygen evolution reaction, Front. Chem. Sci. Eng. 15 (2021) 279–287. https://doi.org/10.1007/s11705-020-1965-2.

[27] L. Jasin Arachchige, Y. Xu, Z. Dai, X.L. Zhang, F. Wang, C. Sun, Double transition metal atoms anchored on Graphdiyne as promising catalyst for electrochemical nitrogen reduction reaction, J. Mater. Sci. Technol. 77 (2021) 244–251. https://doi.org/10.1016/j.jmst.2020.09.048.

[28] Z. Pan, Z. Zhang, A. Tahir, O.C. Esan, X. Liu, H. Wang, L. An, Ultralow loading FeCoNi alloy nanoparticles decorated carbon mat for hydrogen peroxide reduction reaction and its application in direct ethylene glycol fuel cells. Int J Energy Res. 46 (2022) 13820-13831. https://doi.org/10.1002/er.8100.

[29] G. Jerkiewicz, Standard and reversible hydrogen electrodes: theory, design, operation, and applications, ACS Catal. 10 (2020) 8409–8417. https://doi.org/10.1021/acscatal.0c02046.

[30] Y.C. Hao, Y. Guo, L.W. Chen, M. Shu, X.Y. Wang, T.A. Bu, W.Y. Gao, N. Zhang, X. Su, X. Feng, J.W. Zhou, B. Wang, C.W. Hu, A.X. Yin, R. Si, Y.W. Zhang, C.H. Yan, Promoting nitrogen electroreduction to ammonia with bismuth nanocrystals and potassium cations in water, Nat. Catal. 2 (2019) 448–456. https://doi.org/10.1038/s41929-019-0241-7.

[31] W. Xiong, Z. Guo, S. Zhao, Q. Wang, Q. Xu, X. Wang, Facile, cost-effective plasma synthesis of self-supportive FeS: X on Fe foam for efficient electrochemical reduction of N_2 under ambient conditions, J. Mater. Chem. A. 7 (2019) 19977–19983. https://doi.org/10.1039/c9ta07790a.

[32] X. Liu, M. Ouyang, M.W. Orzech, Y. Niu, W. Tang, J. Chen, M.N. Marlow, D. Puhan, Y. Zhao, R. Tan, B. Colin, N. Haworth, S. Zhao, H. Wang, P. Childs, S. Margadonna, M. Wagemaker, F. Pan, N. Brandon, C. George, B. Wu, In-situ fabrication of carbon-metal fabrics as freestanding electrodes for high-performance flexible energy storage devices,

Energy Storage Mater. 30 (2020) 329–336. https://doi.org/10.1016/j.ensm.2020.04.001.

[33] Q. Dai, J. Tang, The optical and magnetic properties of CoO and Co nanocrystals prepared by a facile technique, Nanoscale. 5 (2013) 7512–7519. https://doi.org/10.1039/c3nr01971c.

[34] Y. Liu, Y. Bai, Y. Han, Z. Yu, S. Zhang, G. Wang, J. Wei, Q. Wu, K. Sun, Self-supported hierarchical FeCoNi-LTH/$NiCo_2O_4$/CC electrodes with enhanced bifunctional performance for efficient overall water splitting, ACS Appl. Mater. Interfaces. 9 (2017) 36917–36926. https://doi.org/10.1021/acsami.7b12474.

[35] W. Guo, K. Zhang, Z. Liang, R. Zou, Q. Xu, Electrochemical nitrogen fixation and utilization: Theories, advanced catalyst materials and system design, Chem. Soc. Rev. 48 (2019) 5658–5716. https://doi.org/10.1039/c9cs00159j.

[36] J. Hou, M. Yang, J. Zhang, Recent advances in catalysts, electrolytes and electrode engineering for the nitrogen reduction reaction under ambient conditions, Nanoscale. 12 (2020) 6900–6920. https://doi.org/10.1039/d0nr00412j.

[37] P. Chen, N. Zhang, S. Wang, T. Zhou, Y. Tong, C. Ao, W. Yan, L. Zhang, W. Chu, C. Wu, Y. Xie, Interfacial engineering of cobalt sulfide/graphene hybrids for highly efficient ammonia electrosynthesis, Proc. Natl. Acad. Sci. U. S. A. 116 (2019) 6635–6640. https://doi.org/10.1073/pnas.1817881116.

[38] W. Guo, Z. Liang, J. Zhao, B. Zhu, K. Cai, R. Zou, Q. Xu, Hierarchical cobalt phosphide hollow nanocages toward electrocatalytic ammonia synthesis under ambient pressure and room temperature, Small Methods. 2 (2018) 1–6. https://doi.org/10.1002/smtd.201800204.

[39] F. Lai, J. Feng, X. Ye, W. Zong, G. He, C. Yang, W. Wang, Y.E. Miao, B. Pan, W. Yan, T. Liu, I.P. Parkin, Oxygen vacancy engineering in spinel-structured nanosheet wrapped hollow polyhedra for electrochemical nitrogen fixation under ambient conditions, J. Mater. Chem. A. 8 (2020) 1652–1659. https://doi.org/10.1039/c9ta11408d.

[40] W. Fu, Y. Cao, Q. Feng, W.R. Smith, P. Dong, M. Ye, J. Shen, Pd-Co nanoalloys nested on CuO nanosheets for efficient electrocatalytic N_2 reduction and room-temperature Suzuki-Miyaura coupling reaction, Nanoscale. 11 (2019) 1379–1385. https://doi.org/10.1039/c8nr08724e.

[41] S. Zhang, G. Duan, L. Qiao, Y. Tang, Y. Chen, Y. Sun, P. Wan, S. Zhang, Electrochemical ammonia synthesis from N_2 and H_2O catalyzed by doped $LaFeO_3$ perovskite under mild conditions , Ind. Eng. Chem. Res. (2019). https://doi.org/10.1021/acs.iecr.9b00833.

[42] Y. Wang, X. Cui, J. Zhao, G. Jia, L. Gu, Q. Zhang, L. Meng, Z. Shi, L. Zheng, C. Wang, Z. Zhang, W. Zheng, Rational design of Fe-N/C hybrid for enhanced nitrogen reduction electrocatalysis under ambient conditions in aqueous solution, ACS Catal. 9 (2019) 336–344. https://doi.org/10.1021/acscatal.8b03802.

[43] K. Chu, Y.P. Liu, J. Wang, H. Zhang, NiO nanodots on graphene for efficient electrochemical N_2 reduction to NH_3, ACS Appl. Energy Mater. 2 (2019) 2288–2295. https://doi.org/10.1021/acsaem.9b00102.

[44] X. hu Wang, J. Wang, Y. biao Li, K. Chu, Nitrogen-doped NiO nanosheet array for boosted electrocatalytic N2 reduction, ChemCatChem. 11 (2019) 4529–4536. https://doi.org/10.1002/cctc.201901075.

[45] Y. Chen, B. Wu, B. Sun, N. Wang, W. Hu, S. Komarneni, N-doped porous carbon self-generated on nickel oxide nanosheets for electrocatalytic N_2 fixation with a Faradaic efficiency beyond 30%, ACS Sustain. Chem. Eng. 7 (2019) 18874–18883. https://doi.org/10.1021/acssuschemeng.9b04024.

[46] X. Zhu, J. Zhao, L. Ji, T. Wu, T. Wang, S. Gao, A.A. Alshehri, K.A. Alzahrani, Y. Luo, Y. Xiang, B. Zheng, X. Sun, FeOOH quantum dots decorated graphene sheet: An efficient electrocatalyst for ambient N_2 reduction, Nano Res. 13 (2020) 209–214. https://doi.org/10.1007/s12274-019-2600-8.

[47] X. Zhao, G. Hu, G.F. Chen, H. Zhang, S. Zhang, H. Wang, Comprehensive understanding of the thriving ambient electrochemical nitrogen reduction reaction, Adv. Mater. 33 (2021) 1–46. https://doi.org/10.1002/adma.202007650.

[48] C. Yang, Y. Zhu, J. Liu, Y. Qin, H. Wang, H. Liu, Y. Chen, Z. Zhang, W. Hu, Defect engineering for electrochemical nitrogen reduction reaction to ammonia, Nano Energy. 77 (2020) 105126. https://doi.org/10.1016/j.nanoen.2020.105126.

[49] H. Chen, X. Liang, Y. Liu, X. Ai, T. Asefa, X. Zou, Active site engineering in porous

electrocatalysts, Adv. Mater. 32 (2020). https://doi.org/10.1002/adma.202002435.

[50] D. Ma, Z. Zeng, L. Liu, X. Huang, Y. Jia, Computational evaluation of electrocatalytic nitrogen reduction on TM single-, double-, and triple-atom catalysts (TM = Mn, Fe, Co, Ni) based on graphdiyne monolayers, J. Phys. Chem. C. 123 (2019) 19066–19076. https://doi.org/10.1021/acs.jpcc.9b05250.

[51] M.I. Ahmed, S. Chen, W. Ren, X. Chen, C. Zhao, Synergistic bimetallic $CoFe_2O_4$ clusters supported on graphene for ambient electrocatalytic reduction of nitrogen to ammonia, Chem. Commun. 55 (2019) 12184–12187. https://doi.org/10.1039/c9cc05684j.

[52] J.G. Howalt, T. Bligaard, J. Rossmeisl, T. Vegge, DFT based study of transition metal nano-clusters for electrochemical NH_3 production, Phys. Chem. Chem. Phys. 15 (2013) 7785–7795. https://doi.org/10.1039/c3cp44641g.

[53] E. Skúlason, T. Bligaard, S. Gudmundsdóttir, F. Studt, J. Rossmeisl, F. Abild-Pedersen, T. Vegge, H. Jónsson, J.K. Nørskov, A theoretical evaluation of possible transition metal electro-catalysts for N_2 reduction, Phys. Chem. Chem. Phys. 14 (2012) 1235–1245. https://doi.org/10.1039/c1cp22271f.

[54] B. Ma, H. Zhao, T. Li, Q. Liu, Y. Luo, C. Li, S. Lu, A.M. Asiri, D. Ma, X. Sun, Iron-group electrocatalysts for ambient nitrogen reduction reaction in aqueous media, Nano Res. 14 (2021) 555–569. https://doi.org/10.1007/s12274-020-3049-5.

Figure captions:

Fig. 1. Experimental setup for the electrochemical ammonia synthesis.

Fig. 2. Surface morphology of the FeNi-Co@CM electrode observed by SEM.

Fig. 3. (a-f) High-resolution TEM images of FeNi-Co@CM electrode. (g-i) High-angle annular dark-field (HAADF-STEM) images of FeNi-Co@CM electrode.

Fig. 4. STEM images for elemental mapping by energy-dispersive spectroscopy of FeNi-Co@CM electrode.

Fig. 5. XRD patterns of FeNi-Co@CM electrode.

Fig. 6. XPS spectra of the Co 2p of the FeNi-Co@CM electrode.

Fig. 7. The current density gap between N_2 and Ar bubbling NRR at various potentials (-0.05 V to -0.35 V vs. RHE).

Fig. 8. The ammonia yields and Faradaic efficiency at various potentials.

Fig. 9. The comparable results of our work and other recently reported iron-group electrocatalysts for ambient ammonia synthesis.

Fig. 10. FeNi-Co@CM electrode stability test results.

Fig. 11. Proposed working mechanism of electrocatalytic NRR based on FeNi-Co@CM electrode. (a) Electrode-scale view. (b) Catalyst-scale view. (c) Atomic-scale view.

Table captions:

Table 1 Comparison of our results with other recently reported studies that used iron-group electrocatalysts for ambient ammonia synthesis.

Highlights:

- Achieving an ammonia yield rate of 27.9 μg h^{-1} mg^{-1} and a Faradaic efficiency of 1.52 %
- Demonstrating good stability for 10 cycles by the FeNi-Co@CM electrode
- Revealing the reaction mechanism of NRR from various scales